Modeling of Fouling in Cross-Flow Microfiltration of Suspensions

Nopphon Weeranoppanant
Dept. of Chemical Engineering, Burapha University, Chonburi, Thailand, 20131

Levy I. Amar*
Dept. of Biomedical Engineering, Columbia University, New York, NY, 10027

Evelyn Tong, Monica Faria and Michael I. Hill
Dept. of Chemical Engineering, Columbia University, New York, NY, 10027

Edward F. Leonard
Dept. of Biomedical Engineering, Columbia University, New York, NY, 10027

Dept. of Chemical Engineering, Columbia University, New York, NY, 10027

DOI 10.1002/aic.16412
Published online October 2, 2018 in Wiley Online Library (wileyonlinelibrary.com)

Cross-flow filtration of fine suspensions through microsieves occurs in microprocessing. The interaction of particles with surfaces in microenvironments has been extensively studied, but predominantly in monolayers and not with an eye to microfiltration. Here, we introduce a microfiltration model that pertains to particles that might be seen as fine in a macroscopic environment, but are large enough to intrude significantly into the shear layer of a microchannel. Thus, particle accumulation upon the sieve couples the steady-state filtrate flux and the suspension flow through the microchannel that feeds the sieve. We envision and create a stable, stationary multilayer of particles whose thickness is shear-limited and we identify and verify the structure and parameters that limit steady filtration in this environment. At first, a packed bed of particles forms, growing into and regulated by the micro channel's shear flow. A critical shear stress is shown to determine the thickness of the bed, seen as a stationary and stable multilayer of particles through which filtration may occur. As the bed thickens, at the expense of channel area for suspension flow, surface shear stress increases until no further particle adherence is possible. We built a simple example using hard noninteracting polymer microspheres and conducted cross-flow filtration experiments over Aquamarijn™ microsieves (uniform pore size of 0.8 μm). We observed a steady cake-layer thickness and because of the simple geometry afforded by uniform spheres, we could approximate the force balance, cake resistance, and filtration rate from first principles. The good fit of our data to the proposed mechanism lays a firm basis for the semiquantitative analysis of the behavior of more complex suspensions. © 2018 American Institute of Chemical Engineers *AIChE J*, 65: 207–213, 2019
Keywords: microfiltration, cross-flow, suspension, pore, sieve, packed bed

Introduction

Recently, widespread interest in process intensification has stimulated research into applications of microfluidics for general chemical processing. Cross-flow filtration is a well-established technique that has been used for decades to continuously separate solid-liquid mixtures.[1] While the difficulty of microfluidic solid-liquid separations has been noted,[2-4] there are numerous applications in this environment that could benefit from cross-flow filtration.[5-7] It has been successfully used for bacterial and yeast cell harvesting,[8-11] as plasmapheresis for separating plasma from whole blood,[12,13] for isolating macroscopic quantities of blood components for therapeutic purposes,[14,15] and for nonbiological applications such as waste water recycling and latex separation.[16,17] All of these lead to a filter cake[18] comparable in size to the dimensions of the feed channel.

Despite their potential for widespread industrial and clinical use,[15,19,20] previous models[21-25] for predicting filtrate flux are, in the microfluidic environment, inadequate for explaining experimental observations. Analysis of cross-flow filtration is based on the concept of a stable resistance above that offered by the filter itself,[26] seen as a balance between particles carried to the filter by convection, and opposed by random particle motion expressed as a diffusion-like mechanism.[27] The theory is based on the concept that steady-state filtration is possible only when buildup and removal rates are equal, the classical concentration polarization theory.[28,29] We have found that this theory neither depicts nor explains what is happening in a microchannel, whether filtrating water from spherical particles in aqueous suspension or plasma from red cell suspensions.[12,26,30,31]

With particles that approach the channel size, diffusion is relatively unimportant, and the mechanical interaction of the

Correspondence concerning this article should be addressed to L. Amar at lia2103@columbia.edu

superficial particle layer with the main flow determines a stationary and stable layer.[32,33] Convective diffusion is important only initially, in forming the layer. Particle movements across the cake surface will be directly dependent on the shear rate and permeate flux, as observed and modeled by Knutsen and Davis for both yeast cells and latex microspheres.[26]

In this article, we present a new model based on shear-resistant particle immobilization on the filter surface. Microfluidic cross-flow filtration experiments demonstrate a non-negligible bed of particles building up on a filter surface.[34,35] The layer affects not only the filtrate flux, but also the through flow of retentate.[7,18,36,37] The buildup of particles is rapid, and does not depend upon fouling reactions with the filter surface.[7,38] The model predicts filtration rates when the mechanical interactions among particles, the suspending fluid, and the filtering surface jointly control layer thickness and thus filtration. This model is shown to be in good agreement with experimental data obtained from isometric polymer beads chosen for ease of analysis.

Theory

Filter layers appropriate to microfluidic environments are thin, strong, and highly conductive. Resistance to filtrate flow occurs through a layer of rejected particles; and the resistance of the filter itself is unlikely to control filtrate flow. To simplify the analysis and anticipate corroborating experiments, we begin by assuming that the particle layer to be comprised of hard spheres, all of the same diameter and arranged in multiple layers within the overall filter layer. We assume no adhesive interactions.

When the filter pores have diameters not much less than the spheres above the pores, it is possible for the spheres to be held in place by the pressure differential across the filter. This immobilization will serve to block a certain fraction of the pores, generally less than unity, to a degree that depends on relative diameters, pore spacing, and how the spheres are entrapped. While the net effect of direct pore blockage is to decrease the filter permeability by the fraction of pores blocked, useful filtration often occurs in the presence of a complete particle layer. Uniform spheres will, if randomly layered on a surface until it is "jammed," occupy at their equators 74.77% of the surface (90.69% if in ordered triangular packing). Either way, a layer of spheres leaves room for exposed filter surface because the contact area with the filter is less than the equatorial area to which the given figures apply.

Additional particles may be expected to accumulate over a base layer thus forming a stable, multilayer bed over the filter.[39] A force balance on the layer in contact with the main flow in the microfluidic channel determines the thickness of the aggregate layer. As the overall layer thickens, the channel height remaining for the main flow decreases, and the shear stress on the particle layer increases. The steady channel height is that at which the bed is just able to exert a retaining force on a particle at the interface that is equal to the shear stress imposed on the particle by the main flow. This balance is of interest in microfluidic channels where intrusion of the particle bed into the flow channel is likely to be important.

We predict the critical shear stress, based on the geometry of an ideal isometric spherical particle bed and the filtration rate through the aggregate layer. As shown in Figure 1, components of the vertical and horizontal forces, F_v and F_h, respectively, on a particle held incipiently at the top of the packed bed at an angle of repose α will be equal and opposite. Thus

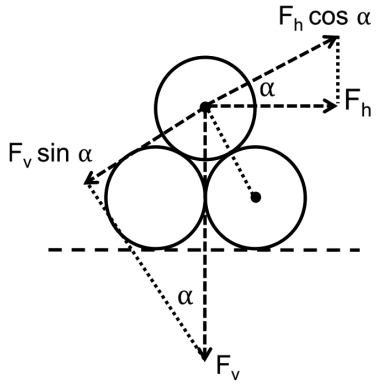

Figure 1. Forces affecting buildup of particles, where F_h is the shear force exerted by the main flow and F_v is the drag force of the filtrate flow.

$$F_h \cos\alpha = F_v \sin\alpha \tag{2.1}$$

Previously, White obtained an empirical expression for the horizontal force F_h, based on studies of erosion of sand beds[28]

$$F_h = 3.4 D_p^2 \tau \tag{2.2}$$

where D_p is the average particle diameter and τ is the shear stress at the top of the bed of particles. We define this stress as the critical shear stress (τ_c), so that

$$F_h = 3.4 D_p^2 \tau_c \tag{2.3}$$

An expression for the vertical force on the particle bed, F_v, may be developed from the Blake-Kozeny equation for flow through packed columns

$$\frac{P_0\text{-}P_L}{L} = 150\frac{\mu\, v_0 (1\text{-}\varepsilon)^2}{{D_p}^2\ \varepsilon^3} \tag{2.4}$$

where P_0 and P_L are the pressures at the top and bottom of the packed column, respectively, μ is the fluid viscosity, v_0 is the fluid superficial velocity, and ε is the void fraction of the bed. Assuming this pressure drop to develop uniformly in the direction of the flow, one obtains

$$-\frac{dp}{dz} = 150\frac{\mu v_0 (1\text{-}\varepsilon)^2}{{D_p}^2\ \varepsilon^3} \tag{2.5}$$

The pressure on the surface of any particle at the top of the bed as a function of position along that particle may be found by describing the particle in spherical coordinates as shown in Figure 2.

$Z = R\cos\theta$, and thus $dz = -R\sin\theta\, d\theta$. Eq. 2.5 then is transformed into

$$\frac{dp}{d\theta} = \frac{75}{D_p}\mu v_0 \frac{(1-\varepsilon)^2}{\varepsilon^3}\sin\theta \tag{2.6}$$

Integrating the resulting ordinary differential equation gives

$$\begin{aligned}\int_{p_0}^{p} dp &= \frac{75}{D_p}\mu v_0 \frac{(1-\varepsilon)^2}{\varepsilon^3}\int_0^{\theta}\sin\theta d\theta \\ &= p(\theta) \\ &= p_0 + 75\frac{\mu v_0}{D_p}\frac{(1-\varepsilon)^2}{\varepsilon^3}\cos\theta - 1\end{aligned} \tag{2.7}$$

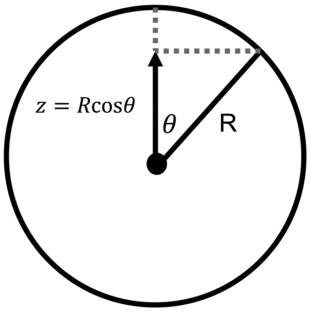

Figure 2. Transformation to spherical coordinates, where $R = D_p/2$.

where p_0 is the pressure at the top of the bed, and θ is an angle measured from a line perpendicular to the plane of the filter and passing through the center of a particle at the fluid surface. The vertical component of the corresponding normal force may be integrated over the entire surface of the particle to find the total vertical force on that particle

$$F_v = \int_0^{2\pi}\int_0^{\pi} (p\cos\theta)\, R^2 \sin\theta\, d\theta\, d\varphi = 25\,\pi\,\mu\, v_0\, D_p \frac{(1-\varepsilon)^2}{\varepsilon^3} \quad (2.8)$$

When the two expressions for F_h and F_v are substituted into the force balance, the critical stress τ_c is found to be

$$\tau_c = \frac{23\,\mu\, v_0}{D_p} \frac{(1-\varepsilon)^2}{\varepsilon^3} \tan\alpha \quad (2.9)$$

For a particle held incipiently at the top of the bed, the critical stress varies with the fluid viscosity, the fluid superficial velocity (which by mass balance must equal the filtrate flux), the packing angle, α (Figure 1), the particle diameter, and the bed porosity. Since fluid viscosity, particle diameter, and packing angle are typically constant for a given system, and the bed porosity will generally be within a narrow range, one expects the critical shear stress to be directly proportional to the filtrate flux. The experiments described below verify this dependence.

Materials and Methods

Preparation of the microsieve

All microsieves were purchased from Aquamarijn, BV, Zutphen, Netherlands as 5 mm by 5 mm silicon nitride microsieves with a uniform pore size of 0.8 μm and a thickness of 700 μm. The controlling flow resistance of the sieves is a layer of silicon nitride approximately 1 μm thick. The perforations are arranged in circles approximately 300 μm in diameter behind which are weep holes that allow filtrate to exit from the opposite side of the sieve. It is necessary to "wet out" the filter to overcome its hydrophobicity. Each sieve was exposed to plasma cleaning (PDC-001-HP [115 V]—Harrick Plasma, Inc., Ithaca, NY) at approximately 200 mTorr for 3 min at 45 W (high-power setting) before assembly to remove surface contamination and render the surface hydrophilic (contact angle <5°) to facilitate wetting. Contact angle measurements were acquired with a contact angle goniometer (Model 200—Ramé-Hart Instrument, Inc., Succasunna, NJ).

Preparation of 5% w/w bead suspensions

Latex microspheres suspensions of two separate diameters (3.2 μm and 7.9 μm) were purchased from Thermo Scientific at 10% w/w concentration. All experiments were conducted with one or the other of these suspensions. The spheres were diluted to 5% w/w with deionized (DI) water and stored at room temperature. Immediately prior to each experiment, the solution was gently inverted to re-suspend the microspheres and was then exposed to a sonicator (Branson 2510, Danbury, CT) for 1 min to dislodge bubbles and break up loose agglomerates.

Microfluidic filter body

The filter body consisted of three layers and three ports, as shown in Figure 3. The bottom metal layer contained the microsieve, mounted in a frame 0.5 mm thick that had been cut from plastic shim-stock (Artus, Englewood, NJ) using cyanoacrylate adhesive (Devcon, Inc.). The middle layer was an open frame cut from 200 μm double-sided tape (ATG type 928 double-sided transfer tape 3M, Minneapolis). The top layer was a clear cover cut from 3 mm polycarbonate sheet stock (McMaster, Inc.). The components were cut to size by a laser cutter (VersaLASER, Scottsdale, AZ).

The device' three ports were designated P1, P2, and P3 (Figure 3). P2 was connected to the feed reservoir containing either filtered water or the bead suspension. Permeate, the portion of liquid feed passing through the filter, flowed from P2 to P1, into a 3 mL syringe whose rate of filling was controlled by a syringe pump (New Era Pump Systems, Wantagh, NY). The remaining fraction of the suspension (i.e., retentate) flowed out of the microchannel through P3 into a 60 mL syringe whose rate of filling was controlled by a similar syringe pump (Harvard Apparatus, Holliston, MA).

After assembling the microchannel, and before attaching the middle and top layers, a test was conducted to ensure that the system was closed. A 3 mL syringe was connected to P1 (Figure 3) and several drops of filtered water were added to cover the entire surface of the microsieve and surrounding white plastic shim. The syringe was pushed inward to see whether bubbles emerged from any of the device' sealed edges. If bubbles appeared, additional cyanoacrylate adhesive was applied. If bubbles were detected on the microsieve, its pore structure was judged to have been breached and was replaced. If no bubbles were seen, the device was judged ready for wetting.

To wet the filter, the 3 mL syringe was pulled outward, so that filtered water flowed through the pores until no further bubbles were seen. After the wetting step, the double-sided tape whose nominal thickness was 200 μm and which had

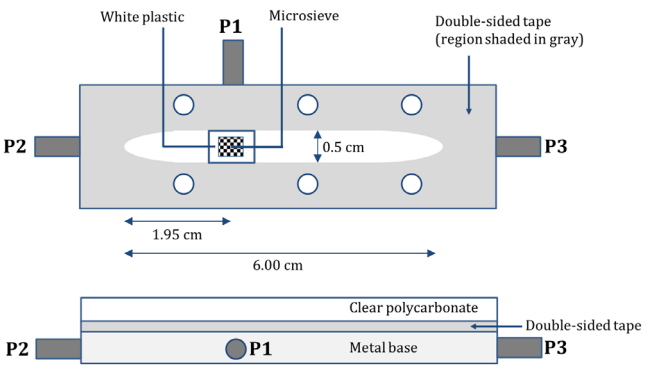

Figure 3. Layout of the microfluidic device, top and side views.

[Color figure can be viewed at wileyonlinelibrary.com]

been cut to the dimensions shown in Figure 3 was attached to the assembly. The clear plastic cover was then attached.

Pressure and transmembrane pressure measurements

The liquid from each port flowed through a pressure sensor (Utah Medical Products, Inc.) connected to a data acquisition card (National Instruments cDAQ-9172, TX) that sent signals to generate the pressure history of each port in a LabView module (National Instruments 9237, TX). The transmembrane pressure (TMP) profile was computed from the three pressure readings in the LabView program using Eq. 3.1

$$\mathrm{TMP} = \left(\mathrm{P}_2 - \frac{1.95}{6.00}(\mathrm{P}_2 - \mathrm{P}_3)\right) - \mathrm{P}_1 \tag{3.1}$$

where P_1, P_2, and P_3 are fluid pressures at ports P_1, P_2, and P_3, respectively. A linear variation of fluid pressure with axial distance along the channel was assumed, and the dimensions shown in Figure 3 were used to estimate the pressure directly above the filter surface.

Permeability of microsieve

Prior to the experiment, the permeability of the filter was determined by the filtration of DI water through the assembly. If the relationship between TMP and filtration rate was linear with a slope less than 11.0 (torr × min/cm^3), the filter was considered to be wetted and fully open.

Calculations

Thickness of the microchannel

The actual thickness of a microchannel was calculated by monitoring pressure drop during the laminar flow of particle-free water assuming the channel to be a narrow slit formed by two parallel walls of width W separated by a distance 2B, and using the slit analog of the Hagen-Poiseuille equation

$$Q_\mathrm{m} = \frac{2(\mathrm{P}_2\text{-}\mathrm{P}_3)B^3 W}{3\mu_\mathrm{w} L} \tag{4.1}$$

The slit height of the microchannel varied from one assembly to another and had to be calculated each time by solving Eq. 4.1 for B[40]

$$B = \left(\frac{3\mu L}{2\frac{\Delta P}{Q_\mathrm{m}} W}\right)^{1/3} \tag{4.2}$$

where Q_m is the main volumetric flow rate, ΔP is the difference between P_2 and P_3, B is the half thickness of the channel, W and L are the width and length of the channel, and μ is the viscosity of the fluid.

Viscosity of particle suspension

The effective viscosity of the particle suspension, μ_s, was determined by solving Eq. 4.1 using the measured pressure drop and the previously determined thickness values of x, B, and W at each Q_m to give

$$\mu_\mathrm{s} = \frac{2B^3 W}{3L}\frac{\Delta P}{Q_\mathrm{m}} \tag{4.3}$$

The ratio $\Delta P/Q_\mathrm{m}$ was employed, as determined from a plot of pressure drop vs. flow in the channel.

Shear stress at the wall

The shear stress exerted at the flow boundaries is calculated as the product of viscosity and the shear rate at the boundaries. The boundary on which filtration occurs extends inward from the filter surface by a distance x, reducing the total slit height to $2B - x$. The shear stresses on each boundary are equal

$$\tau = \mu_\mathrm{s}\gamma = \frac{\mu_\mathrm{s} 3Q_\mathrm{m}}{2\left(B - \frac{x}{2}\right)^2 W} \tag{4.4}$$

Thickness of the particle packed bed

The presence of a packed bed increases the pressure drop along the microchannel. This pressure drop can be written as the sum of three pressure drops for three axial regions: (a) from the inlet to the filter, (b) across the filter, and (c) from the filter to the outlet.

1. When no filtration is applied (and thus no particle layer is formed)

$$\Delta P = \Delta P_\mathrm{a} + \Delta P_\mathrm{b} + \Delta P_\mathrm{c} \tag{4.5}$$

2. During filtration

$$\Delta P' = \Delta P'_\mathrm{a} + \Delta P'_\mathrm{b} + \Delta P'_\mathrm{c} \tag{4.6}$$

where the prime symbols designate the data obtained when filtration is imposed.

Thus, the increase in pressure drop due to a layer of packed bed is estimated by subtracting a pressure drop at no filtration from a pressure drop during filtration. It is assumed that the pressure drop in regions other than the filter surface stay constant ($\Delta P_1 = \Delta P'_1$ and $\Delta P_2 = \Delta P'_2$). Hence the thickness of the packed bed was calculated by solving for x in the following equation

$$\Delta P - \Delta P' = \Delta P_\mathrm{b} - \Delta P'_\mathrm{b} = \frac{3\mu_\mathrm{s} L Q_\mathrm{m}}{2B^3 W} - \frac{3\mu_\mathrm{s} L Q_\mathrm{m}}{2\left(B\text{-}\frac{x}{2}\right)^3 W} \tag{4.7}$$

Results and Discussion

Minimum main flow rate yielding stable TMP at a given filtration flow rate

Steady state is indicated by a stable TMP, and it occurs when components of the shear forceF_h cos α, and drag force, F_v sin α, on the edge of the packed bed are balanced, as described in Eq. 2.1. If the two force components are not balanced, the system remains in a transient state, and the thickness of the bed either increases or decreases, demonstrated experimentally by a changing TMP. As discussed by Aimar et al., variations of permeate flux can significantly alter the condition in the boundary layer.[37] Therefore, in this work we maintained the flux (i.e., the filtration rate) constant and measured TMP. The TMP profile was interrogated to obtain information about the packed bed formation.

We use Q_f to denotate the filtration rate. At each Q_f, a minimum main flow rate $Q_\mathrm{m,min}$ was defined as the lowest value of Q_m to maintain a stable TMP. Figure 4 displays TMP using different Q_m's but a fixed value of Q_f. As shown in Figure 4, at Q_m of 2.000 mL/min, the TMP was unstable, but when Q_m was increased to 2.500 and 3.000 mL/min, the TMP profile leveled off, connotating a stable TMP and steady filtration. Therefore, $Q_\mathrm{m,min}$ was approximated as 2.500 mL/min. The values of $Q_\mathrm{m,min}$ for other conditions (e.g., different bead sizes, Q_f) are summarized in Table 1.

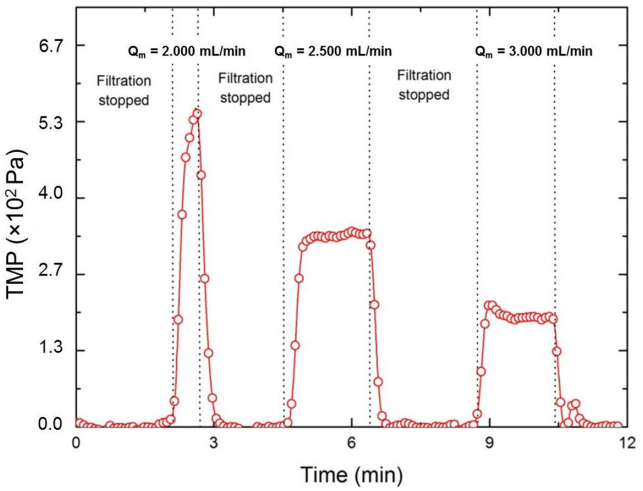

Figure 4. Sample transmembrane pressure profile, given a filtration flow rate of 0.020 mL/min, for various main flow rates (Q_m).

[Color figure can be viewed at wileyonlinelibrary.com]

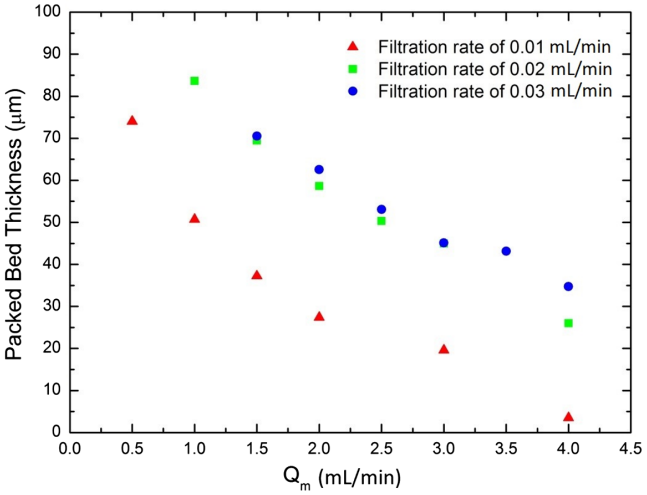

Figure 5. Packed bed thickness as a function of Q_m and Q_f using 7.9 μm bead suspension.

Packed bed thickness decreases as a function of Q_m and increases as a function of Q_f. [Color figure can be viewed at wileyonlinelibrary.com]

As we increase Q_f, $Q_{m,min}$ increases. A higher value of Q_f implies a stronger drag force, which then requires a larger shear force derived from the main flow rate to maintain steady state. $Q_{m,\ min}$ decreases with larger particle sizes. This agrees with expectation that the shear force varies with the square of particle diameter, whereas the drag force is only proportional to particle diameter. Thus, as particle diameter increases, the shear force dominates and requires a smaller $Q_{m,\ min}$ to maintain steady state.

Packed bed thickness and porosity

The packed bed thickness was determined from the difference in channel height (B) without filtration (Eq. 4.1), and with filtration (Eq. 4.7). The assumption here was that for a given Q_m, any change in TMP during filtration was entirely due to the packed bed formation. Eq. 5.1 was used to solve for the effective half-height of the channel in the presence of a packed bed layer,[40] where L is the length of the main channel while x is the thickness of the packed bed

$$\left(B-\frac{x}{2}\right)^3=\frac{3B^3\mu_s LQ_m}{3\mu_s LQ_m-2\left(\text{TMP-TMP}'\right)WB^3} \tag{5.1}$$

The packed bed thickness increases with decreasing Q_m due to a weaker shear force along the channel. We also observed that an increased in Q_f increased the packed bed thickness. This was in agreement with our hypothesis that the drag force would increase the number of particles building up as layers on the filter. However, changes in drag force became less significant when filtration rate (Q_f) was above 0.020 mL/min, as evidenced by similar bed thicknesses at Q_f = 0.020 and Q_f = 0.030 mL/min. At this point, the drag force would lead to denser packing in place of forming more layers. The packed bed thicknesses at different values of Q_f and Q_m are summarized in Figure 5.

For each data set, the Blake-Kozeny calculation of packed bed porosity is applied to test the experimental data. Since the packed bed is incompressible, assuming the porosity to be independent of the imposed differential pressure.[41] The porosity intrinsic to the sphere geometry, ε, is reported to be as 0.35–0.45.[35]

$$\frac{\text{TMP}}{L}=150\left(\frac{\mu_w v_o}{D_p^2}\right)\frac{(1-\varepsilon)^2}{\varepsilon^3} \tag{5.2}$$

Table 2 shows that the porosity obtained from the experimental data set is consistent, and in agreement with the reported value.

Critical shear stress

We define a critical shear stress τ_c, as the minimum sweeping force at the filter surface necessary to prevent formation of the packed bed. If the shear stress exerted by cross-flow filtration is greater than τ_c, no packed bed will form. If the shear stress is smaller than τ_c, the packed bed will build up and narrow the microchannel until the shear stress at the surface of the packed bed is equal to τ_c. At this point, we expect the packed bed to become stable and cease growing.

Table 3 demonstrates the steady state achieved at Q_m of 3.6 mL/min, indicative of the constant wall shear stress at the surface of the packed bed (for 3.2 μm particle size and filtration rate 0.030 mL/min).

Table 1. $Q_{m,min}$ at Different Filtration Rates (Q_f) for Two Different Particle Sizes

	$Q_{m,min}$, mL/min	
Q_f, mL/min	3.2 μm Beads	7.9 μm Beads
0.010	1.500	0.500
0.020	2.500	1.000
0.030	3.500	2.200

Table 2. Calculated Porosity Using the Blake-Kozeny Equation for Q_f = 0.030 mL/min at Varying Q_m

Q_m (mL/min)	Porosity
3.600	0.34
3.700	0.33
3.800	0.33
3.900	0.33
4.000	0.30

Table 3. Calculated Wall Shear Stress of Filtrations at Constant Q_f = 0.030 mL/min for Varying Q_m

Q_m (mL/min)	Wall Shear Stress (Pa)
3.600	4.10
3.700	4.24
3.800	4.11
3.900	4.20
4.000	4.10

Table 4. Average Critical Shear Stress (τ_c) at Different Filtration Rates (Q_f) for Two Different Sizes of Particles Used

	τ_c (Pa)	
Q_f, mL/min	3.2 μm Beads	7.9 μm Beads
0.010	1.50 ± 0.30	0.80 ± 0.23
0.020	3.00 ± 0.89	1.63 ± 0.52
0.030	4.37 ± 1.27	2.47 ± 0.64

The critical shear stress increased with filtration rate. Smaller bead results in higher critical shear stress.

The critical shear stress (τ_c) was calculated using Eq. 4.3. Values of τ_c for two particle sizes (3.2 μm 7.9 μm in diameter) are summarized in Table 4.

Particle size has a large effect on critical shear stress, as evidenced by the critical shear stress for 3.2 μm beads being almost double that for the 7.9 μm beads at the same filtrate flow rate. Another important trend is that the critical shear stress is linearly related to Q_f for the regimen of shear flow analyzed, as shown in Figure 6. It is, thus, possible to predict the critical shear stress given a filtrate flow rate using a linear fit.

A further, qualitative observation corroborates the proposed mechanism and distinguishes it from a diffusion-based explanation of particle accumulation. For the dilute range of particle concentration studied here, there was no effect of particle concentration on the steady-states discussed here and the transitions from one steady state to another were prompt and quicker at higher particle concentrations when layer thickness was increasing because particles were being delivered more quickly. No permanent fouling was observed.

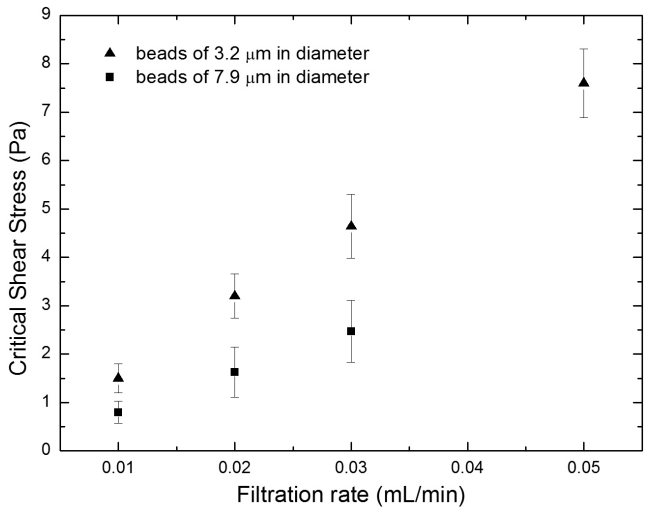

Figure 6. Critical shear stress vs. filtrate flow rate for various bead diameters.

Critical shear stress at each filtration rate (Q_f) was plotted to demonstrate a monotonically increasing trend, aligned with our theoretical prediction.

Conclusion

Cross-flow (tangential) microfiltration of uniform beads in solution can be modeled and interpreted as a simple force balance at the interface between a stationary filter cake and a feed stream moving over it. For a suspension—composed of uniform, hard spherical beads—a first-principles model was built and was successfully compared with experimental data. Other systems may present a more complex interfacial geometry and pore structure. However, such systems should preserve the fundamental findings of this research: that interfacial mechanics, and not particle migration, determine the fraction of a micro filter's cross-section that is available for through-flow.

The essence of this model is that in the crowded space of a microfluidic filter, the feed flows through a narrow slit, sharing the slit height with a stationary filter cake. Thus, a self-sustaining force balance is achieved. This force balance sets and maintains a split in slit height. By measuring TMP for various filtrate and main flow rates, the minimum flow rate and critical shear stress to prevent unstable packed bed formation was found and related to main flow rate, filtrate flow rate, and particle size. A linear relationship was found between critical wall shear stress and filtrate flow rate, an inverse relationship between particle size and critical wall shear stress, and no relationship between the main flow rate and the critical wall shear stress, all in support of the proposed model.

One cannot expect such clear and simple relationships for particles that are more complex in shape and size. However, the underlying phenomenology is likely to be preserved and to provide a basis for understanding and correlating observations in such systems. Further work will be needed to analyze less uniform particle beds.

Acknowledgments

Support for this work was provided in part by Grant 1R21HL088162 from the National Institute of Health, and from Vizio Medical Devices, LLC.

Notation

B	half height of the channel (μm)
D_p	diameter of spherical particles (μm)
F_h	horizontal force on the particle (N)
F_v	vertical force on the particle (N)
L	length of the channel (cm)
ΔP	pressure across the entire channel (Pa)
Q_f	volumetric flow rate of the permeate (i.e., Filtration rate; mL/min)
Q_m	volumetric flow rate along the main channel (mL/min)
$Q_{m,min}$	minimum volumetric flow rate along the main channel required to maintain a stable TMP profile (mL/min)
TMP	transmembrane pressure (Pa)
v_o	filtration velocity or fluid superficial velocity (cm/s)
W	width of the channel (cm)
x	thickness of packed bed (μm)

Greek letters

γ	shear rate (s^{-1})
τ	shear stress (Pa)

τ_c critical shear stress (Pa)
μ viscosity of fluid (Pa.s)
μ_w viscosity of DI water (Pa.s)
μ_s viscosity of bead suspension (Pa.s)
α angle of repose (radian)
ε void fraction of packed bed (%)

Literature Cited

1. Ripperger S, Altmann J. Crossflow microfiltration—state of the art. *Sep Purif Technol*. 2002;26:19-31.
2. Cakl J, Mikulášek P. Flux and fouling in the crossflow ceramic membrane microfiltration of polymer colloids. *Sep Sci Technol*. 1995;30: 3663-3680.
3. Davis RH. Modeling of fouling of crossflow microfiltration membranes. *Sep Purif Methods*. 1992;21:75-126.
4. Gutierrez-Rivera L, Katekawa M, Silva M, Cescato L. Characterization of the selectivity of microsieves using a cross-flow microfiltration system. *Brazilian J Chem Eng*. 2010;27:677-685.
5. Jensen KF. Microreaction engineering—is small better? *Chem Eng Sci*. 2001;56:293-303.
6. Belfort G, Davis RH, Zydney AL. The behavior of suspensions and macromolecular solutions in crossflow microfiltration. *J Memb Sci.* 1994;96:1-58.
7. Di H, Martin GJ, Dunstan DE. A microfluidic system for studying particle deposition during ultrafiltration. *J Memb Sci.* 2017;532:68-75.
8. Tanaka T, Tsuneyoshi S-I, Kitazawa W, Nakanishi K. Characteristics in crossflow filtration using different yeast suspensions. *Sep Sci Technol.* 1997;32:1885-1898.
9. Crespo J, Xavier A, Barreto M, Gonçalves L, Almeida J, Carrondo M. Tangential flow filtration for continuous cell recycle culture of acidogenic bacteria. *Chem Eng Sci*. 1992;47:205-214.
10. Li H, Fane A, Coster H, Vigneswaran S. Observation of deposition and removal behaviour of submicron bacteria on the membrane surface during crossflow microfiltration. *J Memb Sci.* 2003;217:29-41.
11. Wu W-T, Martin AB, Gandini A, Aubry N, Massoudi M, Antaki JF. Design of microfluidic channels for magnetic separation of malaria-infected red blood cells. *Microfluid Nanofluidics*. 2016;20:41.
12. Zydney A, Colton C. Continuous flow membrane plasmapheresis: theoretical models for flux and hemolysis prediction. *ASAIO J*. 1982; 28:408.
13. Zydney A, Colton C. A red cell deformation model for hemolysis in cross flow membrane plasmapheresis. *Chem Eng Commun*. 1984;30: 191-207.
14. Dickson M, Amar L, Hill M, Schwartz J, Leonard E. A scalable, micropore, platelet rich plasma separation device. *Biomed Microdevices*. 2012;14:1095-1102.
15. Malchesky PS. Membrane processes for plasma separation and plasma fractionation: guiding principles for clinical use. *Therapeutic Apher*. 2001;5:270-282.
16. Ahmad AL, Lah C, Fahanis N, Ismail S. Ultrasonically aided crossflow membrane filtration for latex wastewater. *J Phys Sci*. 2018;29: 57-65.
17. Manouchehri M, Kargari A. Water recovery from laundry wastewater by the cross flow microfiltration process: a strategy for water recycling in residential buildings. *J Cleaner Production*. 2017;168:227-238.
18. Di H, Martin GJ, Sun Q, Xie D, Dunstan DE. Detailed, real-time characterization of particle deposition during crossflow filtration as influenced by solution properties. *J Memb Sci.* 2018;555:115-124.
19. Singh V, Purkait M, Das C. Cross-flow microfiltration of industrial oily wastewater: experimental and theoretical consideration. *Sep Sci Technol*. 2011;46:1213-1223.
20. Joshi S, Pellacani P, van Beek TA, Zuilhof H, Nielen MW. Surface characterization and antifouling properties of nanostructured gold chips for imaging surface plasmon resonance biosensing. *Sens Actuators B Chem*. 2015;209:505-514.
21. Bacchin P, Si-Hassen D, Starov V, Clifton MJ, Aimar P. A unifying model for concentration polarization, gel-layer formation and particle deposition in cross-flow membrane filtration of colloidal suspensions. *Chem Eng Sci*. 2002;57:77-91.
22. Zydney A, Colton C. A concentration polarization model for the filtrate flux in cross-flow microfiltration of particulate suspensions. *Chem Eng Commun*. 1986;47:1-21.
23. Vassilieff CS. Convective model of cross-flow microfiltration. *Adv Colloid Interface Sci*. 1992;40:1-36.
24. Mattsson T, Lewis WJ, Chew YJ, Bird MR. The use of fluid dynamic gauging in investigating the thickness and cohesive strength of cake fouling layers formed during cross-flow microfiltration. *Sep Purif Technol*. 2017.
25. Makabe R, Akamatsu K, Nakao S-i. Classification and diafiltration of polydispersed particles using cross-flow microfiltration under high flow rate. *J Memb Sci.* 2017;523:8-14.
26. Knutsen JS, Davis RH. Deposition of foulant particles during tangential flow filtration. *J Memb Sci.* 2006;271:101-113.
27. Belfort G, Davis R, Zydney A. The behavior of suspensions and macromolecular solutions in cross-flow microfiltration. *J Memb Sci.* 1994; 96:1-58.
28. Asaadi M, White D. A model for determining the steady state flux of inorganic microfiltration membranes. *Chem Eng J*. 1992;48:11-16.
29. Davis RH, Sherwood JD. A similarity solution for steady-state crossflow microfiltration. *Chem Eng Sci*. 1990;45:3203-3209.
30. Malchesky PS, Horiuchi T, Lewandowski JJ, Nosè Y. Membrane plasma separation and the on-line treatment of plasma by membranes. *J Memb Sci.* 1989;44:55-88.
31. Makabe R, Akamatsu K, Si N. Limiting flux in microfiltration of colloidal suspensions by focusing on hydrodynamic forces in viscous sublayer. *AIChE J*. 2018;64:1760-1765.
32. Levesley JA, Bellhouse BJ. Particulate separation using inertial lift forces. *Chem Eng Sci*. 1993;48:3657-3669.
33. Wang W, Jia X, Davies GA. A theoretical study of transient cross-flow filtration using force balance analysis. *Chem Eng J Biochem Eng J*. 1995;60:55-62.
34. Tarabara VV, Hovinga RM, Wiesner MR. Constant transmembrane pressure vs. constant permeate flux: effect of particle size on crossflow membrane filtration. *Env Eng Sci*. 2002;19:343-355.
35. Smith WO, Foote PD, Busang PF. Packing of homogeneous spheres. *Phys Rev*. 1929;34:1271-1274.
36. Mackley MR, Sherman NE. Cross-flow cake filtration mechanisms and kinetics. *Chem Eng Sci*. 1992;47:3067-3084.
37. Aimar P, Howell JA, Turner M. Effects of concentration boundary-layer development on the flux limitations in ultrafiltration. *Chem Eng Res Design*. 1989;67:255-261.
38. Song L. Flux decline in crossflow microfiltration and ultrafiltration: mechanisms and modeling of membrane fouling. *J Memb Sci*. 1998; 139:183-200.
39. Losey MW, Schmidt MA, Jensen KF. Microfabricated multiphase packed-bed reactors: characterization of mass transfer and reactions. *Industrial Eng Chem Res*. 2001;40:2555-2562.
40. Bird RB, Stewart WE, Lightfoot EN. *Transport Phenomena*. New York: Wiley; 2007.
41. Lightfoot EN. *Transport phenomena and living systems; biomedical aspects of momentum and mass transport*. New York: Wiley; 1973.

Manuscript received May 24, 2018, and revision received Sep. 5, 2018.